Supporting Information

In Situ Construction of Dual Network Binder Synergistically Enables the Stability of SiO Anodes

Siyi Jing[1, a], *Weihua Wang*[1, a], *Yudai Huang*[*, a], *Wenyi Li*[a], *Haozhe Liu*[a], *Wei Wang*[a], *Xueyan Ma*[a], *Yingde Huang*[b], *Chengwei Fan*[*, c], *Letao Zhang*[*, c], *Zhouliang Tan*[*, a]

[a] State Key Laboratory of Chemistry and Utilization of Carbon-Based Energy Resources, College of Chemistry, Xinjiang University, Urumqi, 830017, China

[b] School of Materials Science and Engineering, Zhengzhou University, Zhengzhou, 450001, China

[c] School of Chemistry and Environmental Engineering, Xinjiang Institute of Engineering, Urumqi, 830029, China

[1] These authors contributed equally to this work.

[*]Corresponding authors.

E-mail addresses:

huangyd@xju.edu.cn (Y. Huang); tzl6880@xju.edu.cn (Z. Tan); fcw_upc@163.com (C. Fan); zhangletao2004@163.com (L. Zhang)

Experimental Section

Materials:

Silicon monoxide (SiO 200 nm, 99.99%) was purchased from Nangong Bole Metal Materials Co., Ltd. Tapioca starch (TA, containing 80% branched starch and 20% linear starch) was supplied by Xinliang Group. Fumaric acid (FA) was sourced from Fuchen Chemical Reagent Co., Ltd. Sodium alginate (SA, analytical grade), polyvinylidene fluoride (PVDF) and carboxymethyl cellulose (CMC) were purchased from Shanghai Aladdin Biochemical Technology Co., Ltd. $LiNi_{0.8}Co_{0.1}Mn_{0.1}O_2$ (NCM811) cathode material was supplied by Shanghai Ziyi New Energy Technology Co., Ltd. Both electrolytes LX-025 (for silicon-carbon systems) and LX-032 (for ternary systems) were purchased from Suzhou Duoduo Chemical Technology Co., Ltd.

Preparation of TA-FA/SiO:

Dissolve 36.4 mg TA and 3.6 mg FA in distilled water, stirring at room temperature for 30 min to form a homogeneous solution. Add 120 mg SiO particles, continue stirring for 30 min, then transfer to a 110 ℃ oil bath for 80 min of in situ cross-linking. Subsequently, 40 mg of acetylene black was added to form a uniform slurry with a solid mass ratio of SiO: acetylene black: TA-FA = 6:2:2. Spread the slurry onto copper foil, air-dry for 6 h, then vacuum-dry at 80°C for 12 h. The electrodes were finally punched into 12 mm diameter discs with an active material loading of approximately 0.4-1.1 mg cm^{-2}.

Fabrication of Half and Full Cells:

CR2032 coin cells were assembled in an argon-filled glove box (H_2O, O_2 < 0.01 ppm). Celgard 2400 was used as the separator, with metallic lithium as the counter electrode. The electrolyte (LX-025) (1 M $LiPF_6$ in EC/DMC/DEC (1:1:1, v/v/v) with 10 vol% FEC) was used in the half cell

tests. For the full cell tests, a commercial electrolyte (LX-032) of 1.0 M $LiPF_6$ in EC: DEC (1:1, v/v) with 10 wt. % FEC was used. A precise volume of 90 μL was injected into each CR2032 coin cell. The full cell employs a pre-lithiated TA-FA/SiO anode (pre-lithiation conditions: 3 cycles at 0.2 A g^{-1} current density) and an NCM811 cathode, with LX-032 selected as the electrolyte.

Electrochemical Test:

Batteries were tested after 12 h of equilibration. A Land system was used for constant-current charge/discharge and GITT testing. Half-cell voltage range was 0.01-1.5 V, with activation at 0.2 $A \cdot g^{-1}$ for 3 cycles followed by high-current performance evaluation. The full cell was cycled between 2.6-4.3 V. After activation at 0.1 C, long-term cycling was performed at 0.2 C (1 C = 200 mA g^{-1}). CV tests were conducted at 0.1-0.9 $mV \cdot s^{-1}$ within 0.01-1.5 V. EIS measurements were performed at frequencies ranging from 200 kHz to 10 mHz with an amplitude of 10 mV.

Material Characterization:

Fourier Transform Infrared Spectroscopy (FTIR, INVENIO R, Bruker, USA) was employed to analyze chemical bond structures; tensile properties were tested at a rate of 20 $mm \cdot min^{-1}$ using a universal testing machine (ZQ-990L, ZhIQU, China); rheological behavior was characterized via a rotational rheometer (HAAKE MARS60+iS50, Thermo Fisher Scientific, USA). Mechanical properties were tested using a nanoindenter (Nano Indenter G200, KLA, USA) at a maximum load of 1000 μN; a video optical contact angle meter was employed to evaluate the wettability between the binder and electrodes; Thermal stability of TA-FA was evaluated using a thermogravimetric analyzer (TGA, SDT650/DSC300, TA, USA); X-ray diffraction (XRD, SmartLab SE, Rigaku, Japan) analyzed the SiO crystal structure; Field emission scanning electron microscopy (SEM, (SEM, GeminiSEM 500, ZEISS, Germany)) was observed electrode surface morphology; Triple ion beam

cutter (EM TIC 3X, Leica, Germany) processed cross-sections, with thickness variations characterized using GeminiSEM 500 (ZEISS, Germany). X-ray photoelectron spectroscopy (XPS, K-Alpha, Thermo Scientific, USA) analyzed post-cycle electrode surface elements; Transmission electron microscopy (TEM, JEM-F200, JEOL, Japan) was observed the SEI film structure of SiO particles, combined with energy dispersive spectroscopy (EDS) for elemental analysis; atomic force microscopy (AFM, Dimension Icon, Bruker, Germany) to measure surface roughness, Young's modulus, and energy dissipation in quantitative nanomechanical mode.

Theory Calculation:

Random SiO particles of varying sizes were embedded into composite materials using two types of binders. COMSOL Solid Mechanics and the Third Current Module were employed to simulate the stresses experienced by SiO particles during lithiation. Dilute mass transfer followed the Fick's diffusion law, with ion intercalation modeled through free diffusion within the solid. The stress-concentration coupling was achieved by simulating concentration-dependent intercalation strain.

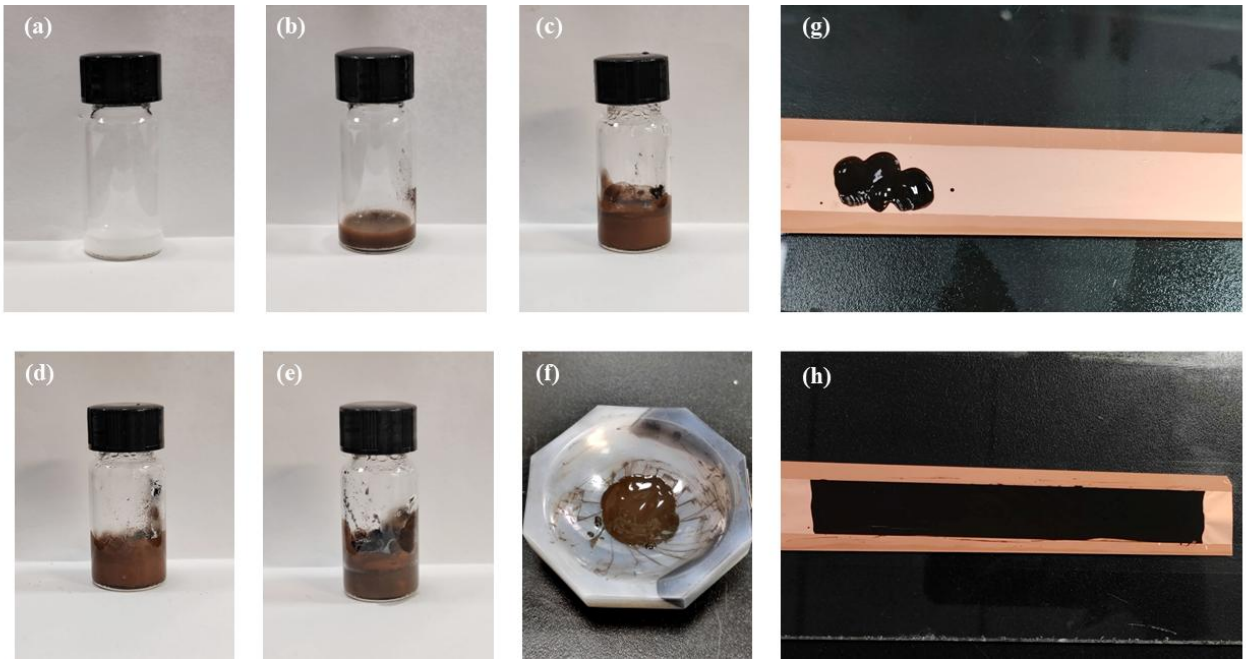

Fig. S1. Preparation process of TA-FA/SiO.

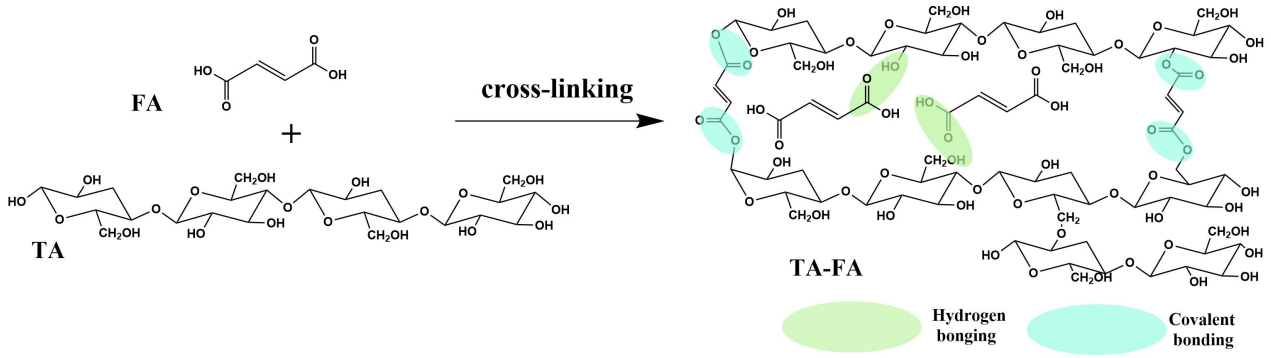

Fig. S2. Schematic diagram of the preparation of the TA-FA binder.

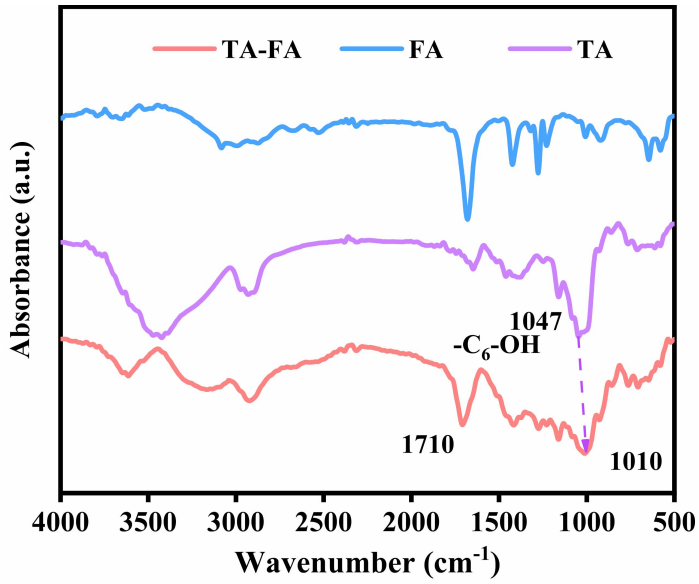

Fig. S3. FTIR spectra of TA, FA, and TA-FA.

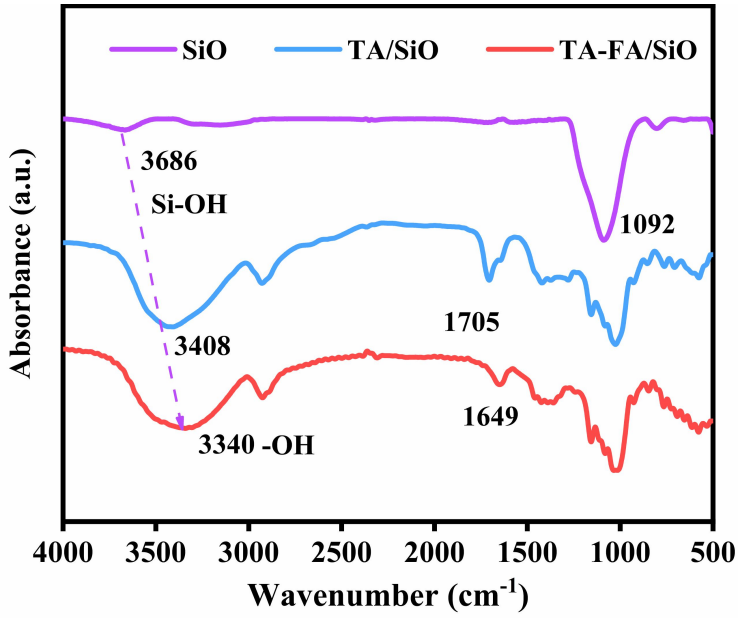

Fig. S4. FTIR spectra of SiO, TA/SiO, and TA-FA/SiO.

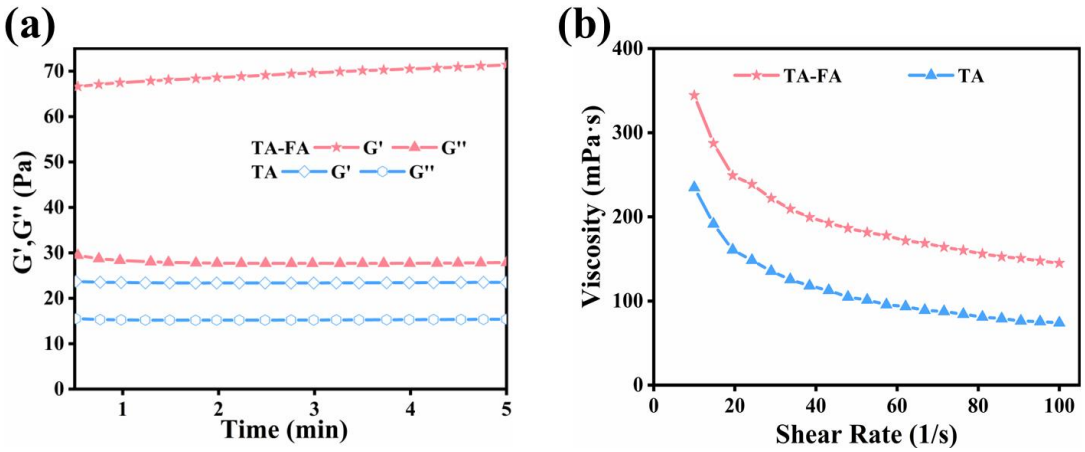

Fig. S5. (a) Time-scan measurements of TA and TA-FA at 25 °C (G′: elastic modulus, G″: viscous modulus). (b) Dynamic viscosity tests of TA and TA-FA at different shear rates.

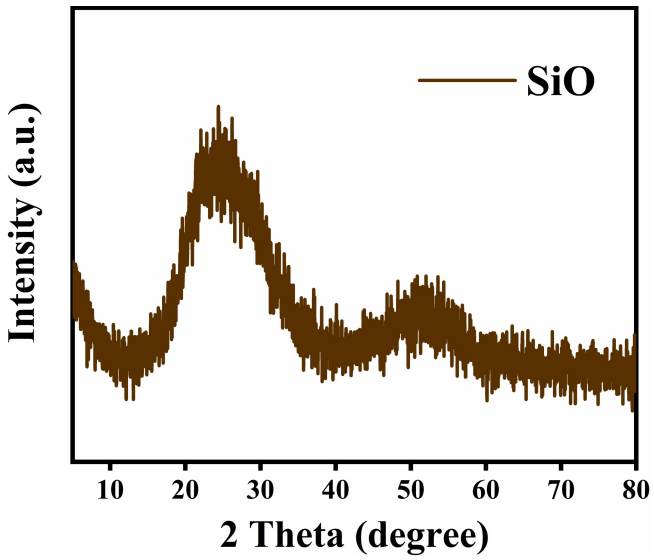

Fig. S6. The XRD pattern of SiO.

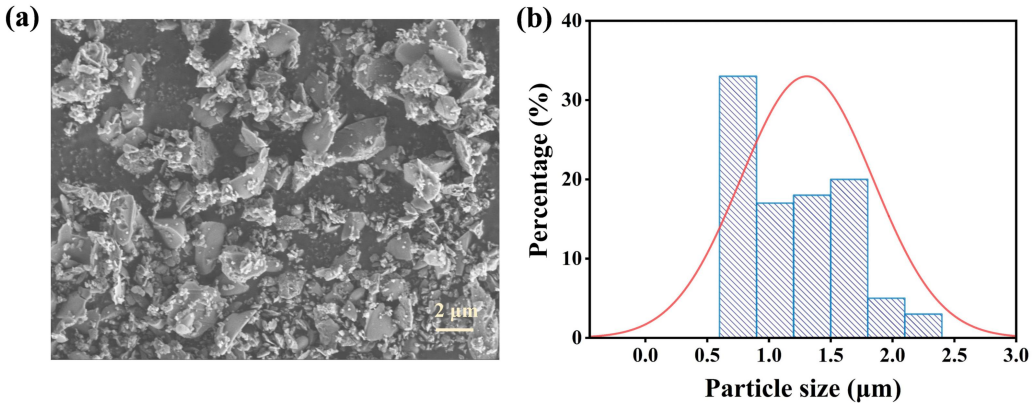

92

93 **Fig. S7.** (a) SEM image of SiO particles and (b) particle size distribution.

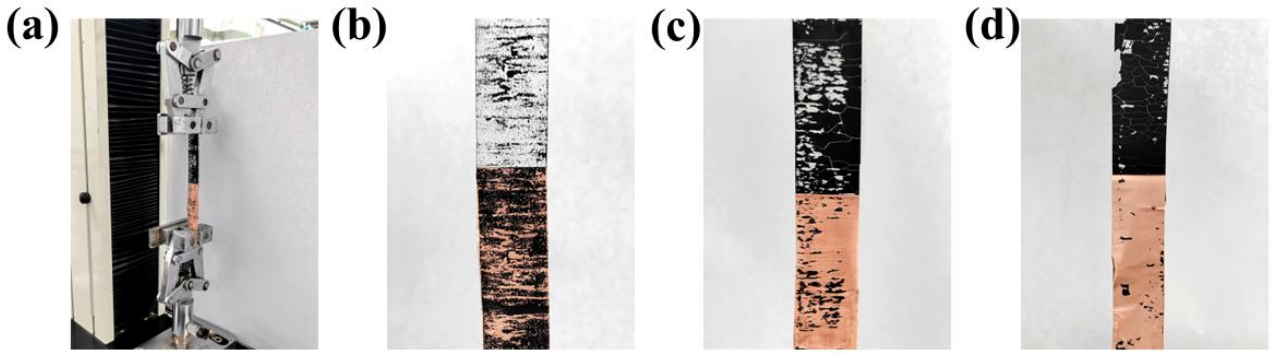

Fig. S8. Digital photographs of different electrodes after 180°peeling tests: (a) peeling machine, (b) TA-FA/SiO, (c) TA/SiO, and (d) SA/SiO.

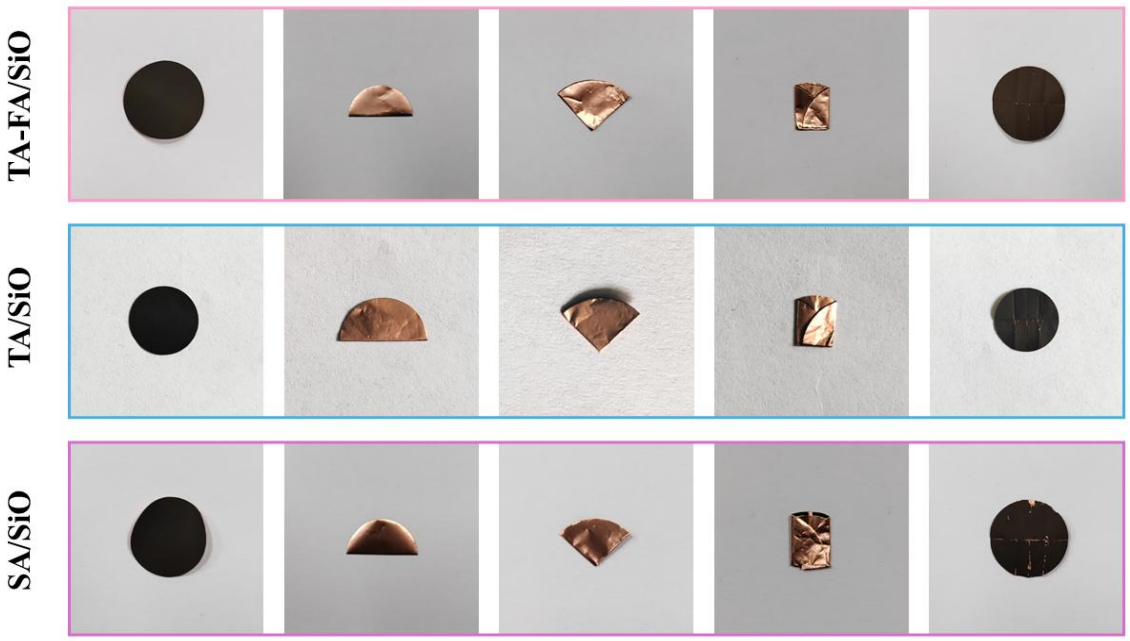

Fig. S9. Digital photographs of TA-FA/SiO, TA/SiO, and SA/SiO during the folding experiment.

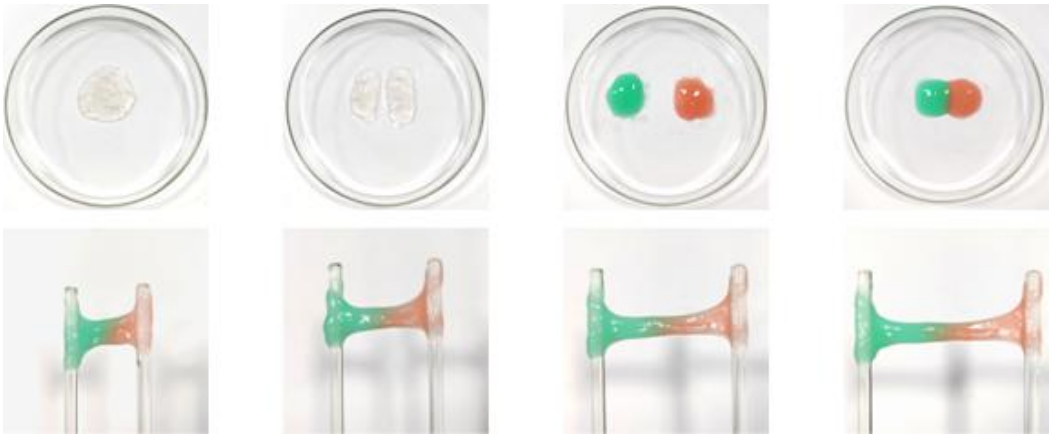

Fig. S10. Self-healing capability demonstration of the TA-FA binder.

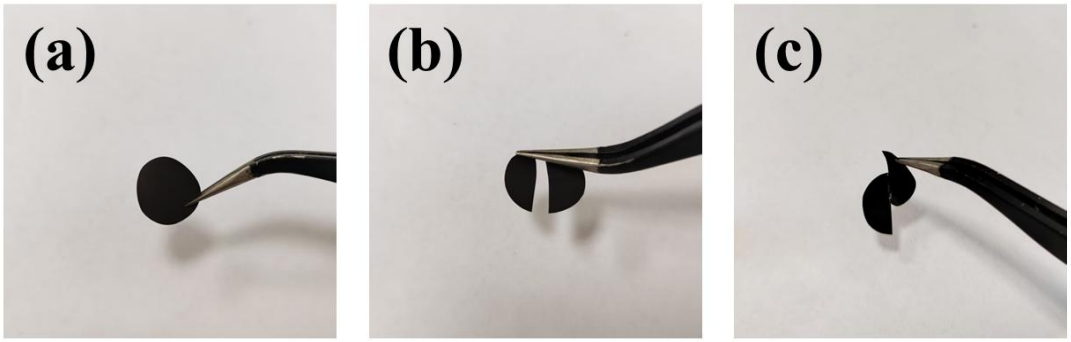

Fig. S11. Digital photographs of TA-FA/SiO electrodes (a) initial, (b) cut in half, and (c) self-healed.

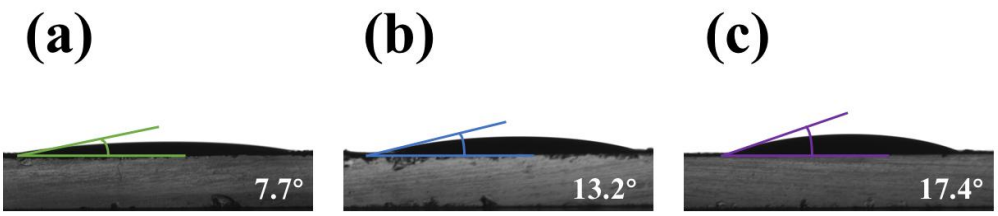

Fig. S12. Contact angle test digital photographs of different SiO electrodes and organic electrolytes: (a) TA-FA/SiO, (b) TA/SiO, and (c) SA/SiO.

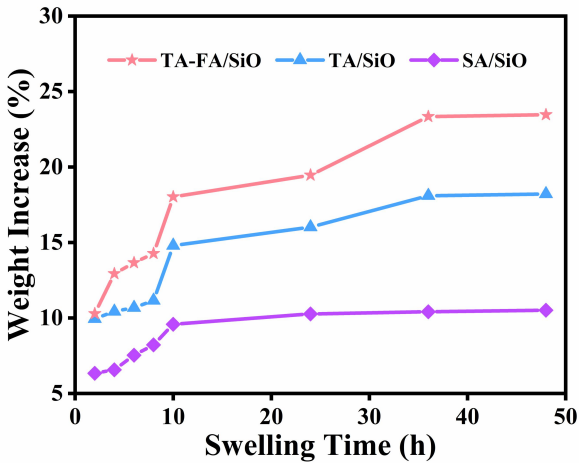

Fig. S13. Electrolyte swelling behavior of different SiO electrodes.

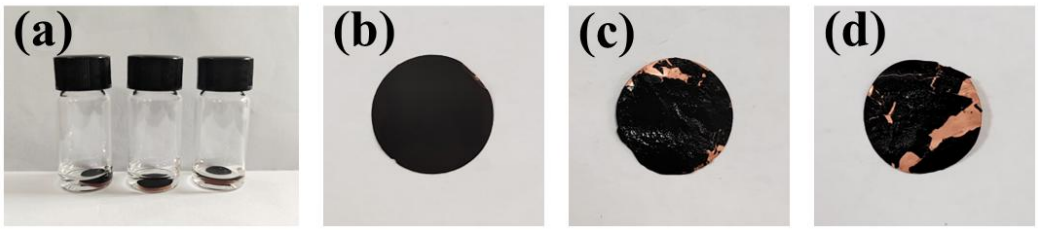

Fig. S14. Different electrode immersion experiments: (a) Immersion digital photographs of different electrodes after 20 days of immersion, (b) TA-FA/SiO, (c) TA/SiO, and (d) SA/SiO.

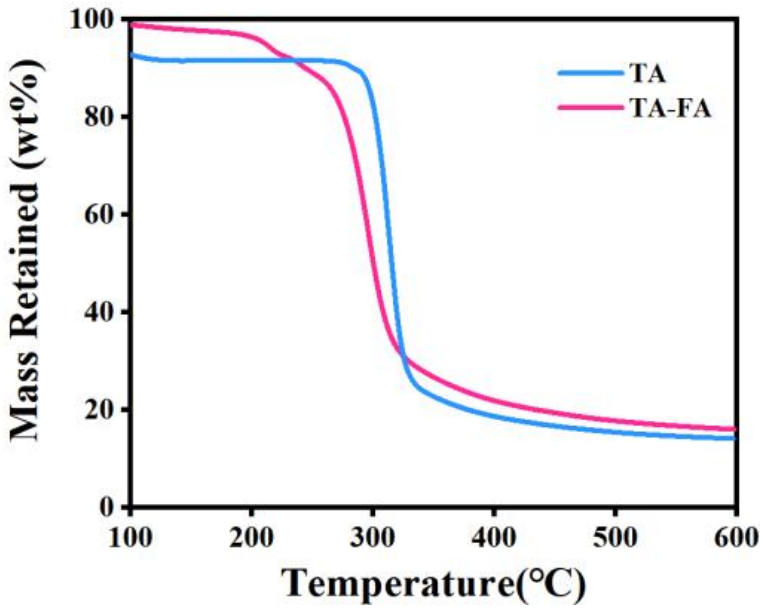

Fig. S15. TGA testing of TA and TA-FA.

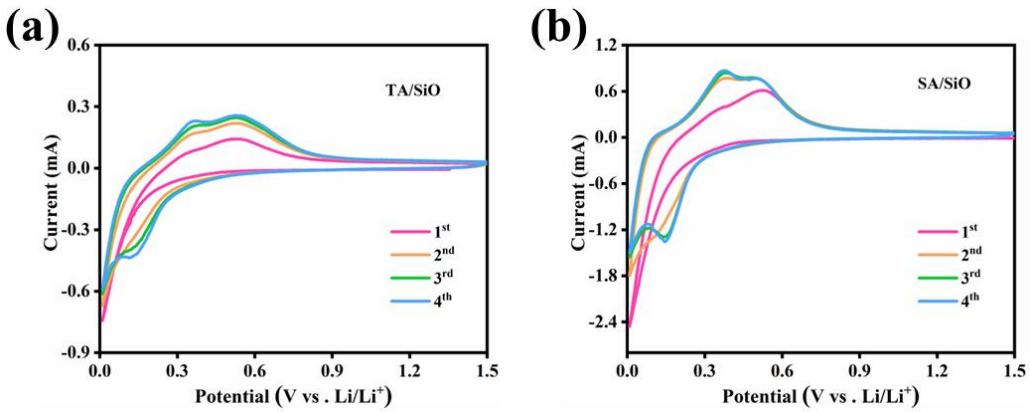

Fig. S16. CV curves at scan rate of 0.1 mV s^{-1}: (a) TA/SiO and (b) SA/SiO.

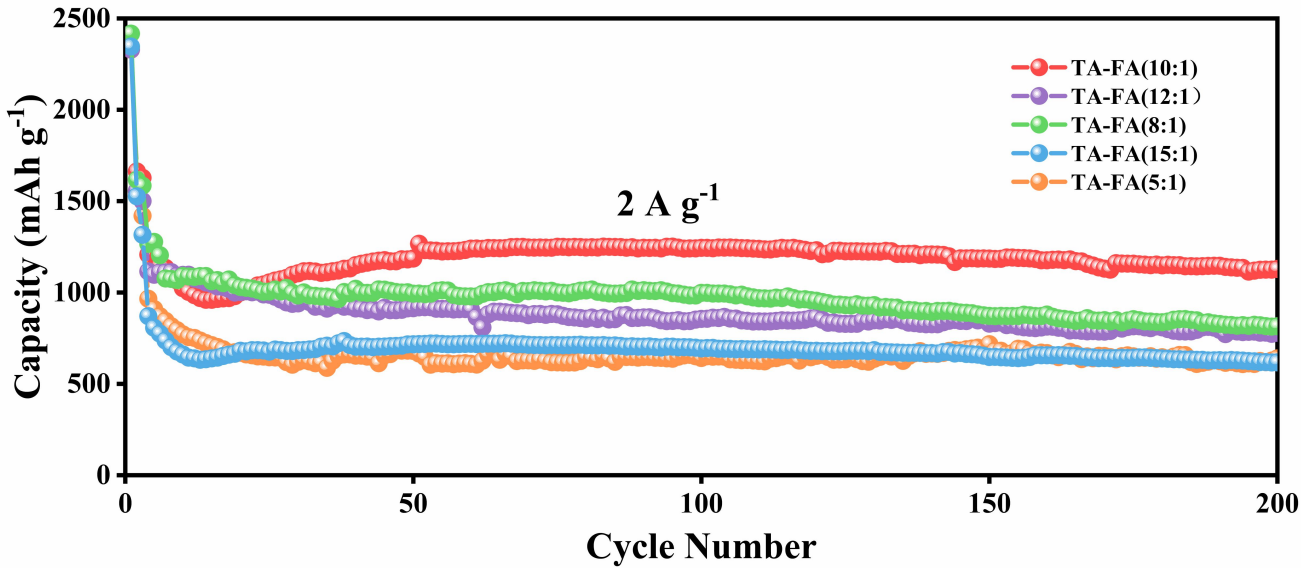

116

117 **Fig. S17.** Cycling performance of TA-FA/SiO with different mass ratios at 2 A g^{-1}.

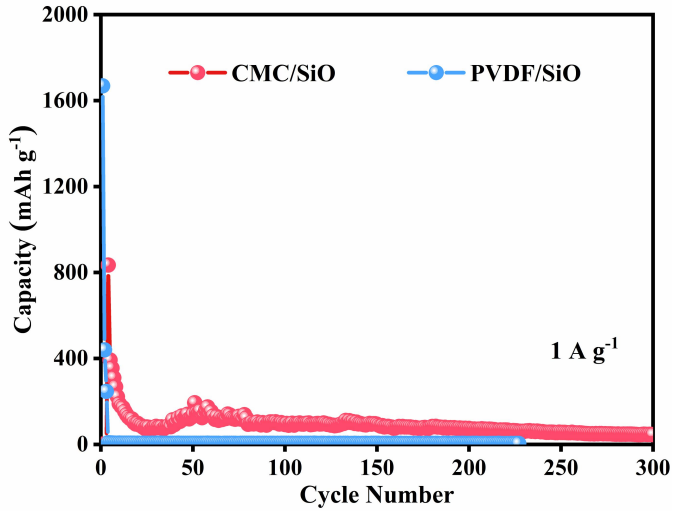

118

119 **Fig. S18.** Cycling performance of PVDF/SiO and CMC/SiO at 1 A g^{-1}.

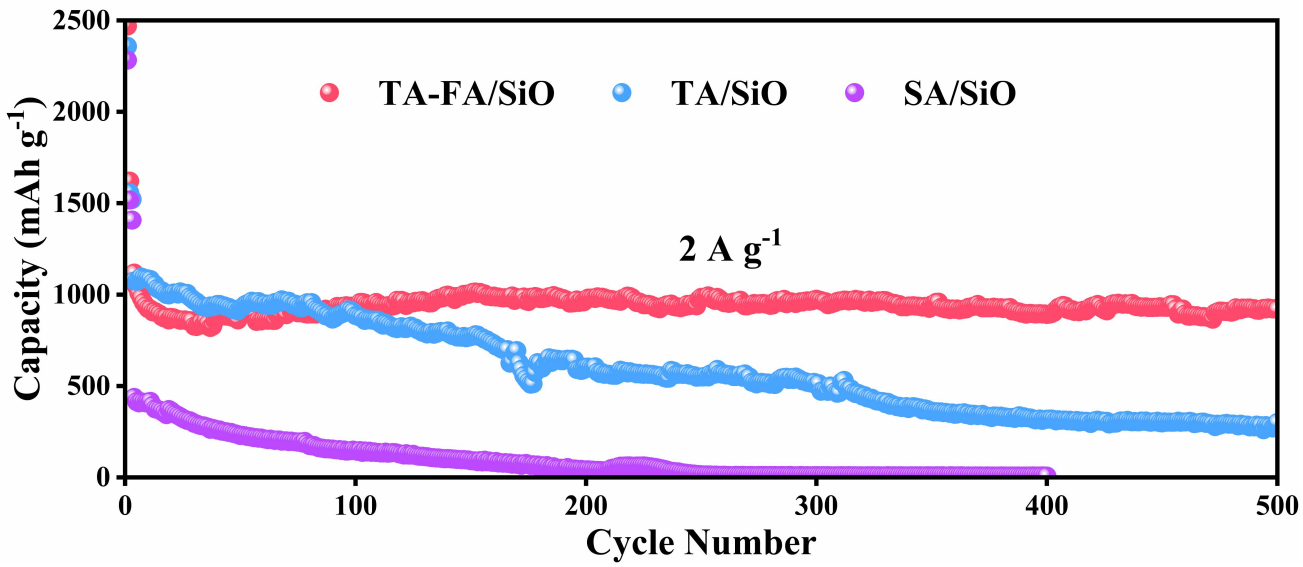

Fig. S19. Cycling performance of TA-FA/SiO, TA/SiO, and SA/SiO at 2 A g^{-1}.

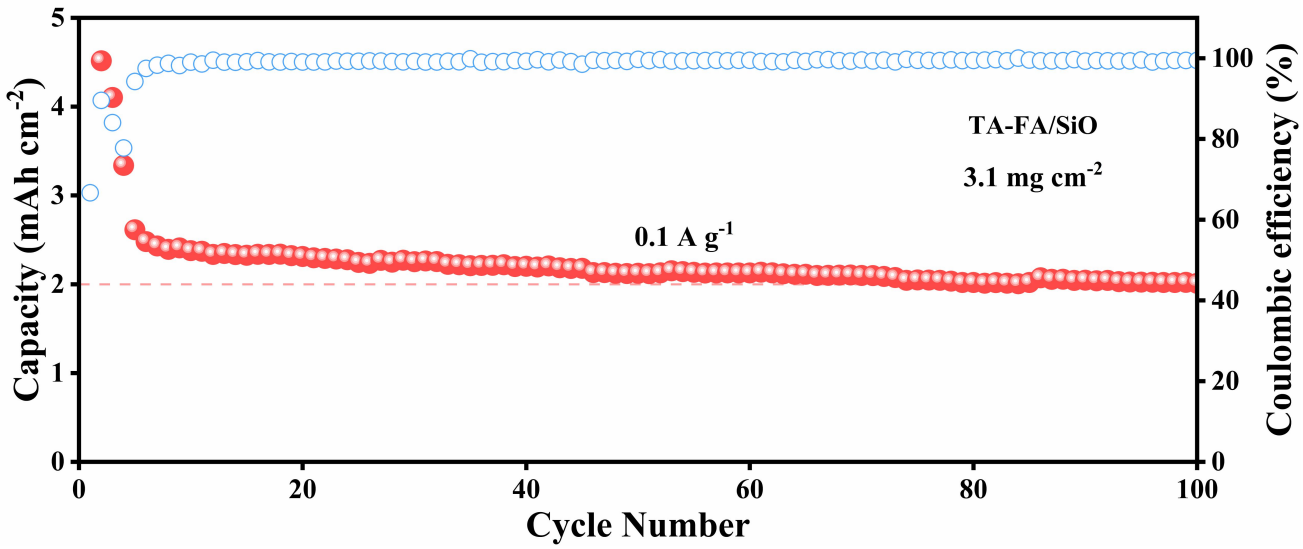

Fig. S20. Cycling performance of highly loaded TA-FA/SiO at 0.1 A g^{-1}.

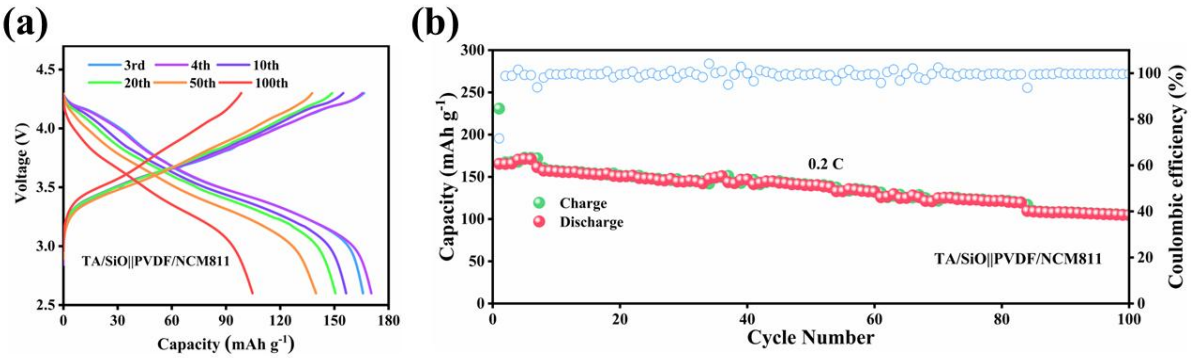

Fig. S21. (a) Charge/discharge curves of different cycle numbers and (b) cycling performance of TA/SiO||PVDF/NCM811 full cell at 0.2 C.

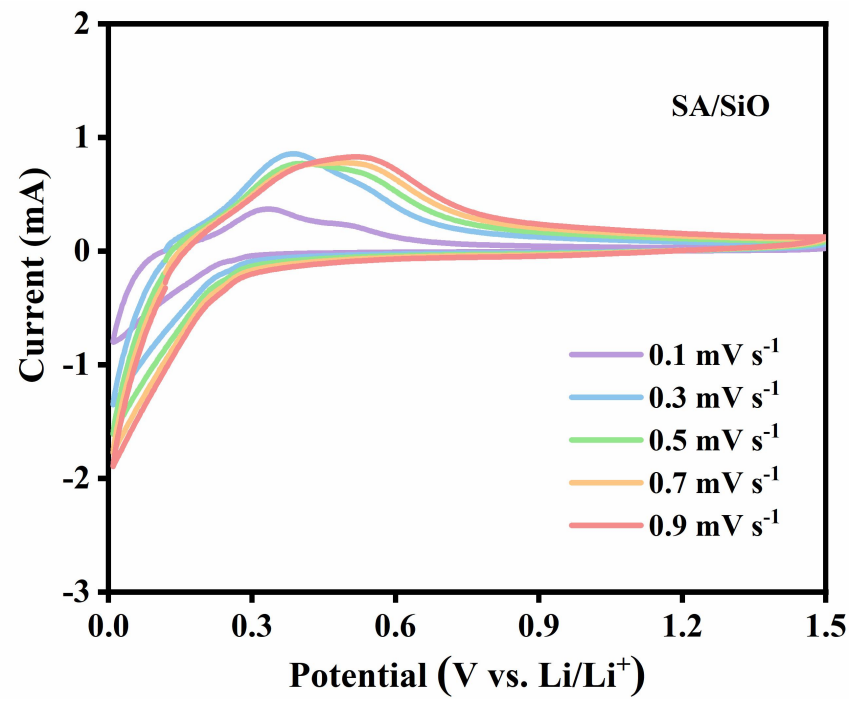

127

128 **Fig. S22.** CV curves of SA/SiO at different scan rates (0.1 to 0.9 mV s^{-1}).

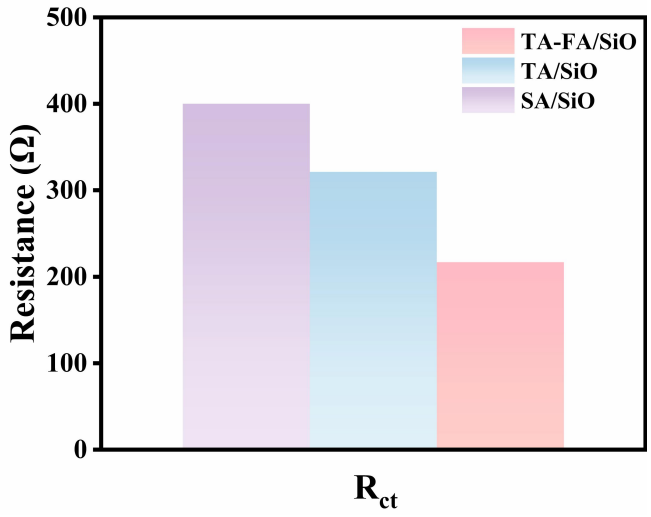

129

130 **Fig. S23.** R_{ct} of SiO electrodes with different binders before cycling.

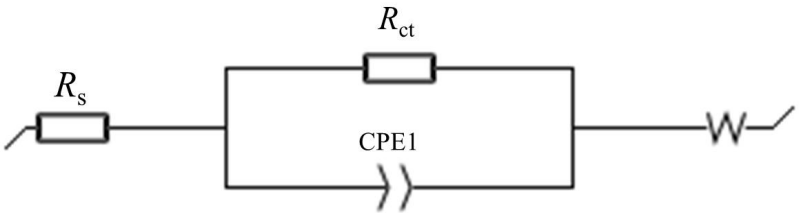

Fig. S24. Equivalent circuit model before cycling.

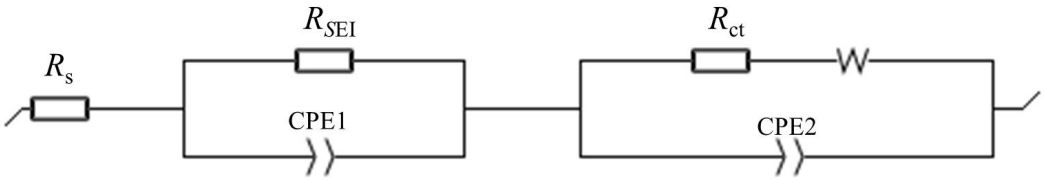

Fig. S25. Equivalent circuit model after cycling.

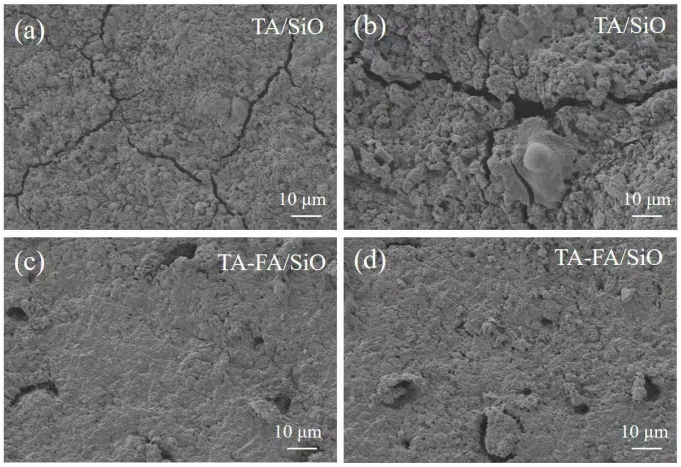

Fig. S26. SEM images after 20 cycles: (a) TA/SiO and (c) TA-FA/SiO. SEM images after 50 cycles: (b) TA/SiO and (d) TA-FA/SiO.

Fig. S27. Digital photographs of electrodes (a) TA-FA/SiO, (b) TA/SiO, and (c) SA/SiO after 300 cycles.

Table S1. Comparison of the cycling performance of TA-FA/SiO and previously reported SiO electrodes with different binders.

Samples	Current density ($A\ g^{-1}$)	Cycle number	Capacity ($mAh\ g^{-1}$)	Refs.
TA-FA/SiO	**1.0**	**300**	**921.6**	**This work**
	2.0	**500**	**919.6**	
$SiO@PAA_{10}$-PTA_1+1%Fe^{3+}	0.5	500	884.8	*Chem. Eng. J.*, 2024, **499**, 156360
SiO_x@PG82	0.5	350	975.0	*Ind. Eng. Chem. Res.*, 2025, **64**, 14141-14149
SiO_x@GG-PAA	1.0	150	882.2	*J. Power Sources*, 2025, **642**, 236961
SiO_x@P(AA-co-LiAMPS)	0.65	400	587.8	*Small Sci.*, 2023, **4**, 2300133
SiO_x@PAA-Dex_9	1.0	300	607.0	*ACS Appl. Mater. Interfaces*, 2023, **15**, 10726-10734
SiO_x@CMC-PA	0.5	200	671.0	*Macromol. Chem. Phys.*, 2022, **223**, 2200068
SiO_x/PGA-ECH	0.5	500	900.0	*ACS Appl. Mater. Interfaces*, 2022, **14**, 18625-18633
SiO_x@P31	0.65	300	734.0	*ACS Appl. Mater. Interfaces*, 2022, **14**, 42494-42503
SiO_x@CS-EDTA	1.0	200	721.0	*ACS Appl. Mater. Interfaces*, 2022, **5**, 4788-4795
SiO_x@c-CMC-IDA_{150}	1.0	200	899.0	*ACS Appl. Mater. Interfaces*, 2021, **13**, 49313-49321
SiO_x/PSP663	0.5	300	770.0	*ACS Appl. Mater. Interfaces*, 2019, **11**, 26038-26046

Table S2. Comparison of the rate performance (maximum current density) between TA-FA/SiO and SiO electrodes using previously reported binders.

Samples	Current density (A g^{-1})	Capacity (mAh g^{-1})	Refs.
TA-FA/SiO	**5.0**	**522.4**	**This work**
SiO@SA-$LiCl_{40}$	3.0	468	*J. Power Sources*, 2026, **663**, 238904
SiO_x/C@PIHB-450	4.05	＜100	*Polymer*, 2025, **333**, 128664
SiO_x@CMC-PA	2.0	507.4	*Macromol. Chem. Phys.*, 2022, **223**, 2200068
SiO_x/C@LBG@XG	2.0	＜300	*ACS Appl. Mater. Interfaces*, 2023, **15**, 49071-49082
SiO_x/G@C-PAA	1.6	219	*Mater. Chem. Phys.*, 2022, **292**, 126797
SiO_x/C@PSAP663	1.2	238	*ACS Omega*, 2021, **6**, 26805-26813
SiO_x/C-B	5.0	224.9	*Chem. Select*, 2023, **8**, e202300233

Table S3. Comparison of the cycling performance between the assembled full cell using TA-FA/SiO and the previously reported assembled full cell using SiO electrodes with different binders.

Samples	Current density (C)	Cycle number	Capacity ($mAh\ g^{-1}$)	Capacity retention rate (%)	Refs.
TA-FA/SiO//NCM811	**0.2**	**100**	**147.9**	**92.8**	**This work**
SiO@SA-$LiCl_{40}$//NCM811	0.3	50	＜100	_	*J. Power Sources*, 2026, **663**, 238904
SiO_x@PG82//NCM622	0.5	100	141	86	*Ind. Eng. Chem. Res.*, 2025, **64**, 14141-14149
SiO_x@PAA-Dex_9//$LiCoO_2$	0.2	100	90	_	*ACS Appl. Mater. Interfaces*, 2023, **15**, 10726-10734